Computer-Assisted Segmentation of Videocapsule Images Using Alpha-Divergence-Based Active Contour In The Framework of Intestinal Pathologies Detection

Leila Meziou, Aymeric Histace, Frédéric Precioso, Olivier Romain, Xavier Dray, Bertrand Granado, Bogdan Matuszewski

Computer-Assisted Segmentation of Videocapsule Images Using Alpha-Divergence-Based Active Contour In The Framework of Intestinal Pathologies Detection

L. Meziou[a], A. Histace[a], F. Precioso[b], O. Romain[a], X. Dray[a, c], B. Granado[d], B.J. Matuszewski[e]

[a]ETIS, Université de Cergy-Pontoise, ENSEA, CNRS, Cergy, France
[b]I3S, Université de Nice/Sophia-Antipolis, CNRS, Antibes, France
[c]Paris Sorbonne Paris 7 University & APHP, Hôpital Lariboisière, Paris, France
[d]LIP6, Université Pierre et Marie Curie, CNRS, Paris, France
[e]ADSIP Research Centre, School of Computing, University of Central Lancashire, Preston, UK

Abstract
Visualization of the entire length of the gastrointestinal tract through natural orifices is a challenge for endoscopists. Videoendoscopy is currently the "gold standard" technique for diagnosis of different pathologies of the intestinal tract. Wireless Capsule Endoscopy (WCE) has been developed in the 1990's as an alternative to videoendoscopy to allow direct examination of the gastrointestinal tract without any need for sedation. Nevertheless, the systematic post-examination by the specialist of the 50,000 (for the small bowel) to 150,000 images (for the colon) of a complete acquisition using WCE remains time-consuming and challenging due to the poor quality of WCE images. In this article, a semiautomatic segmentation for analysis of WCE images is proposed. Based on active contour segmentation, the proposed method introduces alpha-divergences, a flexible statistical similarity measure that gives a real flexibility to different types of gastrointestinal pathologies. Results of segmentation using the proposed approach are shown on different types of real-case examinations, from (multi-) polyp(s) segmentation, to radiation enteritis delineation.

Keyword: Videocapsule, Active Contour, Alpha-Divergence, Gastrointestinal Pathologies

Address all correspondance to: Aymeric Histace, ENSEA/ETIS, 6 av. du Ponceau, CS 20707 CERGY, 95014 Cergy-Pontoise Cedex, France, Tel: +33134256834, aymeric.histace@u-cergy.fr

1 Introduction

Visualization of the entire length of gastrointestinal tract through natural orifices is a challenge for endoscopists. Moreover, radiologic techniques are relatively insensitive for diminutive, flat, vascular, or inflammatory lesions of the small bowel. Currently, videoendoscopy is the "gold standard" technique for the diagnosis of various gastrointestinal diseases. Noticeably, using a videoendoscope, gastroenterologists can perform and record a complete examination of the colon, aiming to detect, to characterize, to sample, and to remove suspicious tissular structures like adenomas (pre-neoplastic lesions from which colorectal cancer can emerge). In most cases, videocolonoscopy is performed under general anaesthesia. Alternatively, mini-invasive techniques such as computed-tomography-based colonography and Wireless Capsule Endoscopy (WCE) have been proposed when sedation is contra-indicated or refused. In this article, we focus our attention on WCE devices.

Since 1994 [Moglia 09], WCEs have been developed to allow direct visualization of the small bowel (a hardly accessible part of the gastrointestinal tract) without any need for sedation. Small bowel WCE are best indicated for obscure gastrointestinal bleeding, for evaluation of Crohn's disease and coeliac disease, and when small bowel polyposis (Peutz-Jeghers syndrome) or tumors are suspected. The Pillcam© video capsule designed by Given Imaging Company is the most popular of them (see Fig. 1 for illustration).

PillCam©	Endocapsule©	Mirocam©	Omom©
			

Fig. 1 Illustration of the existing WCE devices

This autonomous device images the gastrointestinal tract during at least 8 hours. However, acquired images are of low resolution and imaging conditions are sometimes very poor, as the movements, the speed of the WCE, and the illumination, are not entirely controlled (see Fig. 2 for illustration). Moreover a complete acquisition is made of more than 50,000 images for the small bowel (and up to 150,000 for colon WCE), and the analysis of such an amount of data is therefore demanding and tedious for physicians. Image segmentation and analysis would be of great interest to decrease the physician's workload.

Fig. 2 Three images extracted from three different video made with a Pillcam© WCE (taken from the freely available database "Gastro Vidéo Web" (http://dr.dm.gastro.free.fr/).

However, segmentation of WCE images is a challenging problem with two main issues:

1. A substantial reducing of the initial 50,000+ images to analyse is necessary since a lot of them do not show meaningful information from a clinical standpoint, and, consequently do not need to be analysed.
2. The development of an (semi-) automatic segmentation approach to robustly and precisely delineate detected structure for further characterization (size, shape, texture for instance) is a real need from a Computer-assisted diagnostic perspective.

Regarding the first issue, in [Silva, 14], we proposed an automatic boosting-based detection approach for abnormal Region of Interest (ROI) identification, with a particular focus on polyp detection. A database of 500 polyps and 1200 non-polyps was used to learn by boosting the optimal classifier in terms of false positive (FP) and true positive (TP) rates. In this study, texture parameters were used (computed from the co-occurrence matrix) and a global detection rate of 94% was reached with a FP rate of 4%. This work, achieved on classic videoendoscopic images, is currently being extended to other type of structure than polyps and to WCE images, for which the image database is far more difficult to enrich because of limited access to raw images data. Fig. 3 displays three examples of obtained results. In each case, non-bold squares show candidate regions *before* the classifying step, whereas the bold square shows the region eventually identified as a polyp using the boosted classifier. It is important to highlight here that a resolution of only 5 bits (32 grey-levels) was used to compute the co-occurrence matrices from which the Haralick's parameters are then computed. It shows that even for low-resolution WCE images (with respect to classic resolution of videocolonoscopy images), the method remains adapted.

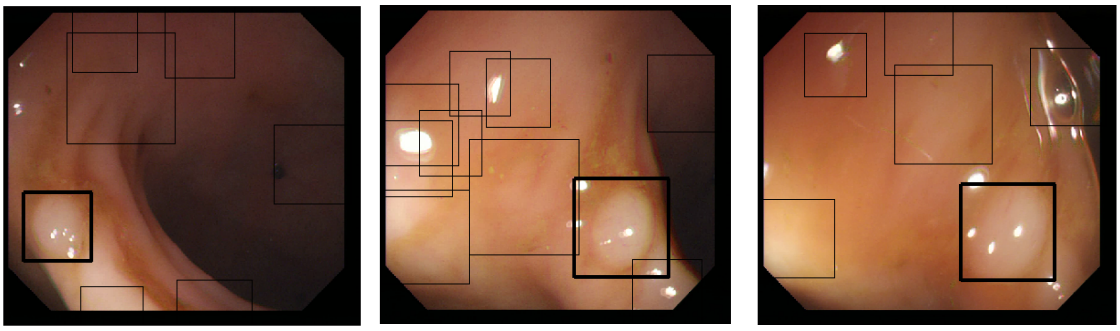

Fig. 3 Three examples of the proposed boosting-based polyp detection approach in [Silva 14]

To illustrate this, Fig. 4 shows a detection/recognition obtained on one of the WCE images of Fig. 2 without any learning step dedicated to WCE images[1].

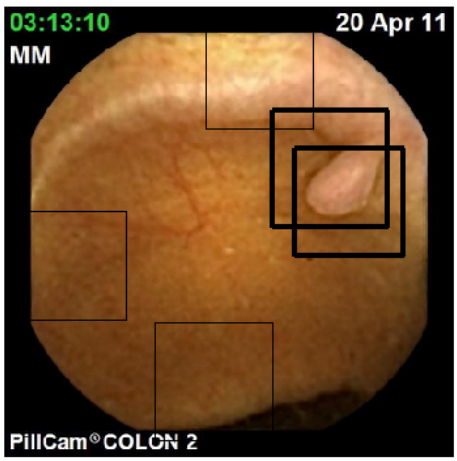

Fig.4 Detection and recognition of a polyp area using the approach proposed in [Silva 14] on a WCE images. It can be noticed, that the only 5-bits resolution of the co-occurrence matrices used for the learning step of the algorithm, avoid to be too dependant of the "quality" of the image.

Starting from these results, a fine segmentation is required to address the second issue mentioned above. In this article, a method for WCE-image-segmentation based on statistical active contours is proposed and a prospective study on various types of gastrointestinal structures is presented.

The remainder of this article is divided into 4 sections: Section 2 introduced the data considered and their specificity in terms of illustrated pathology. Section 3 is focused on the theoretical aspect of the segmentation method proposed; Mainly a recall on histogram-based active contour is first presented and the details on the developed method follow. Segmentation

[1] Currently, most of the WCE companies use a patented codec for the encryption of the videos which makes quite hard the gathering of a sufficient amount of images to create a database with a significant amount of WCE images.

experiments on synthetic images and WCE images are shown in Section 4; the objective of this section is, firstly, to evaluate the method on controlled set-ups (noise and texture) and secondly to show comparative performance on the particular targeted clinical application. Finally Conclusion and Discussion are proposed in Section 5.

2 Materials

Images used for the study purpose were acquired using the PillCam© device and were taken from the freely available database "Gastro Vidéo Web" (http://dr.dm.gastro.free.fr/). Resolution of images is 320x320 pixels.

To show the flexibility of the proposed active contour approach, different segmentation tasks were considered including some demanding ones. Nine conditions selected for the study (Fig. 9): gastric polyps (a, b), colon sigmoid polyp (c), lymphangiectasia (d), small-bowel metastasis (e), radiation enteritis (f), angiodysplasia (g), lipoma (h), and hypertrophied anal papilla (i).

In each case, the segmentation task consisted in delineating, with precision and reproducibility, the structure of interest in order to estimate clinical parameters.

3 Method

3.1 Main principle and notations

Among the existing proposed segmentation methods in medical imaging, active contour models have attracted extensive research in the past two decades. Originally proposed in 1988 [Kass 88], the basic idea of the active contour is to iteratively evolve an initial curve towards the boundaries of target organ driven by the combination of internal forces determined by the geometry of the evolving curve and the external forces induced from the image (see Fig. 5 for illustration). Image segmentation method using active contour is usually based on minimizing a functional, which is so defined that for curves close to the target boundaries it has small values. The minimization process is iteratively performed until convergence is reached i.e. the value of the computed energy does not meaningfully change from an iteration to the following one. In the following, we will refer to the active contour and the related evolution equation using the notation of Eq. (1) and Eq. (2).

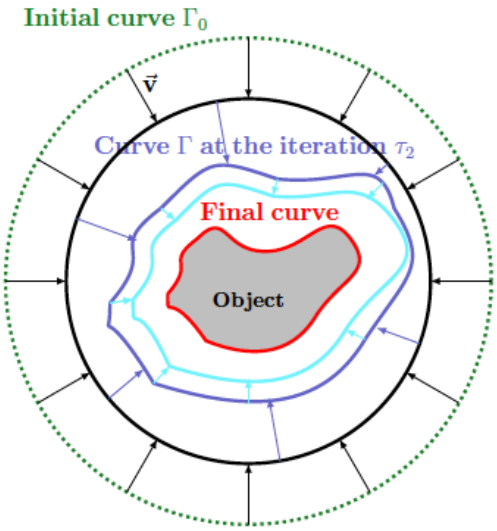

$$\begin{cases} [a,b]\times[0,T] \rightarrow \Re^2 \\ (p,\tau) \rightarrow \Gamma(p,\tau) = \mathrm{x}(p,\tau) = \begin{pmatrix} x(p,\tau) \\ y(p,\tau) \end{pmatrix} \end{cases} \quad (1)$$

$$\begin{cases} \dfrac{\partial \Gamma(p,\tau)}{\partial \tau} = v(p,\tau) \\ \Gamma(p,0) = \Gamma_0(p) \end{cases} \quad (2)$$

Fig. 5 Illustration of active contour segmentation: $\Gamma = \Gamma(p, \tau)$ denotes the coordinate of the point p of the curve at iteration τ of the segmentation process.

Former gradient-based approaches have been now beneficially replaced since the early twenties by region-based approaches that are less sensitive to the initialization of the curve, less sensitive to noise and more stable in terms of obtained results. In that category, the classic Chan and Vese [Chan 01] approach is the most used in image segmentation.

Nevertheless, in the particular context of medical image segmentation, the Chan and Vese approach does not suit to the particular acquisition noise and more generally to the particular imaging conditions: this can be explained by the strong hypothesis of Gaussianity of the luminance distribution law of the inner and outer region of the active curve which is definitely not the case when considering WCE images for instance. For illustration, Fig. 6 shows the luminance distribution function associated to a polyp segmentation task. In blue the inner probability density function (PDF) is shown (p_{in}), and in red the outer PDF (p_{out}). As it can be noticed, the PDFs do not compel with the hypothesis of Gaussianity. In that particular context, histogram-based active contour approaches are of better interest than classic region-based ones.

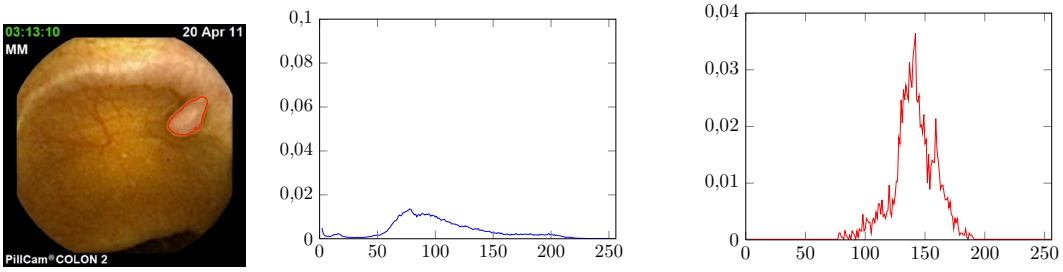

Fig. 6 Illustration of the non-Gaussianity of the PDF (luminance) extracted from a WCE image presenting with a polyp. Left: delineation of the polyp, middle: inner PDF of the luminance (polyp), right: outer PDF (background).

3.2 Alpha-divergence

In the particular framework of histogram-based active contour segmentation [Aubert03, J-Besson 03, Herbulot 07, Lecellier 10, Lecellier 14], external forces involve optimization of distance (or divergence) between the luminance PDF computed from the inner (p_{in}) and the outer (p_{out}) regions delimited by the boundaries of the active curve. If usually the Kullback-Leibler (KL) divergence is used, as shown in [Hero06], when inner and outer PDF have too strong overlapping, KL-divergence may fail in separating the two PDF.

To overcome the limitations of KL-divergence, a particular statistical distance is proposed: the alpha (α)-divergence. This similarity measure is a generalization of the KL-divergence, which becomes an asymptotic case (α tends to one) of the alpha-divergence. Main advantage of proposed approach is the flexibility of the alpha-divergence which metric can be adapted to very difficult PDF separation tasks [Hero06].

In the following, $D_\alpha(.\|.)$ will denote the alpha-divergence defined by:

$$D_\alpha\left(p_{in}\,\|\,p_{out}\right)=\int_{\Re^m}\varphi_\alpha\left(p_{in},p_{out},\lambda\right)d\lambda \qquad (3)$$

with φ_α the corresponding alpha-metric such as:

$$\varphi_\alpha\left(p_{in},p_{out},\lambda\right)=\begin{cases}\dfrac{\alpha p_{in}+(1-\alpha)p_{out}-p_{in}^{\alpha}p_{out}^{1-\alpha}}{\alpha(1-\alpha)}, & \alpha\in\Re\setminus\{0,1\}\\ p_{out}\log\left(\dfrac{p_{out}}{p_{in}}\right)+p_{in}-p_{out}, & \alpha=0\\ p_{in}\log\left(\dfrac{p_{in}}{p_{out}}\right)+p_{out}-p_{in}, & \alpha=1\end{cases} \qquad (4)$$

In Eq (3), λ is the grey-level resolution of the image (i.e. in our case $\lambda \in [0,255]$).

In Eq. (3) and Eq. (4), it can be noticed that for particular values of α, some usual distances of the literature can be related to alpha-divergences. For instance,

$$\begin{cases} D_2\left(p_{in} \,\|\, p_{out}\right) = \frac{1}{2} D_{\chi^2}\left(p_{in} \,\|\, p_{out}\right) \\ D_{0.5}\left(p_{in} \,\|\, p_{out}\right) = 2 D_{Hellinger}\left(p_{in} \,\|\, p_{out}\right) \\ D_{KL}\left(p_{in} \,\|\, p_{out}\right) = \lim_{\alpha \to 1} D_\alpha\left(p_{in} \,\|\, p_{out}\right) \end{cases} \quad (5)$$

where $D_{KL}(.\|.)$ is the KL-divergence.

As stated before, this makes alpha-divergence a generic divergence estimation, with multiple tuning possibilities via alpha parameter and, as a consequence, a very flexible measure in the context of non-Gaussian PDF characterizing inner and outer regions delimited by the active curve all along the segmentation process.

3.3 PDF modeling

Practically speaking, the use of alpha-divergence in the framework of histogram-based active contour requires the estimation of the inner and outer PDF. More precisely, the fact that Eq. (4) will be optimized using an Euler-derivative approach imposes a continuous and derivable formulation of the PDF. Classically, two kinds of approaches are considered: a parametric estimation or a non-parametric one. In the first case, the PDF can be analytically expressed as part of a general family like the exponential one. Nevertheless, it can be seen as a limitation since in practical medical case, PDF can be of very complex shapes (see Fig. 5 for instance) that cannot be easily expressed in a particular statistical family.

The second solution proposes to estimate the PDF using a Gaussian-mixture model based on Parzen-window estimator [Parzen 62]. The PDF is then given by:

$$p_i\left(I(x,y), \Omega_i\right) = \frac{1}{|\Omega_i|} \int_{\Omega_I} g_\sigma\left(I(x,y) - \lambda\right) d\lambda \quad (6)$$

with $i \in [in, out]$, Ω_i representing all the pixels of region i and g_σ a Gaussian kernel function of standard deviation σ.

Such approach does not limit the type of PDF to be estimated and compel with the requirement of class C^1. Such properties definitely fit with our context of applications and in the following Parzen Window technique is used.

3.4 Alpha-divergence-based active contour

As explained above, the segmentation task is formulated as an optimization problem. More precisely, a maximisation of Eq. (3) using the classic "shape gradients" framework formerly proposed in [Auber03] leads to the following evolution equation, as shown in [Meziou 12], for non parametric estimation of the PDF using Parzen window technique:

$$\frac{\partial \Gamma}{\partial \tau} = \left[\frac{1}{|\Omega_{in}|}(A_1 - C_1) - \frac{1}{|\Omega_{out}|}(A_2 - C_2) \right] \mathrm{N} \tag{7}$$

with

$$\begin{aligned} A_j &= \partial \varphi_\alpha \left(p_{in}, p_{out}, \lambda \right) * g_\sigma \left(I(\mathrm{x}) \right) \\ C_j &= \int_{\Re} \partial_j \varphi_\alpha \left(p_{in}, p_{out}, \lambda \right) p_i \, d\lambda \end{aligned} \tag{8}$$

where $\{i, j\} = \{\{in,1\},\{out,2\}\}$, $\partial_1 \varphi_\alpha$ and $\partial_2 \varphi_\alpha$ are the derivatives of φ_α with respect to the first (p_{in}) and the second (p_{out}) variable, and * denotes the convolution operator.

4 Results

4.1 Implementation

In order to be able to segment images presenting multiple target objects, we propose to embed the alpha-divergence maximization within the classic level-set framework [Osher 88].

Moreover, because a regularization of the obtained curve is needed not to take into account to small regions in the final segmentation result, a minimisation of the final length of the curve is added to Eq. (7). Considering the classic level-set embedding function $\Phi : \Re^2 \times \Re \to \Re$, the final evolution equation is then given by:

$$\frac{\partial \Phi}{\partial \tau} = \delta\Phi \left[\beta . \nabla . \left(\frac{\nabla \Phi}{|\nabla \Phi|} \right) - \xi . \left(\frac{1}{|\Omega_{in}|}(A_1 - C_1) - \frac{1}{|\Omega_{out}|}(A_2 - C_2) \right) \right] \tag{9}$$

with β and ξ two weighting parameters, $\delta(.)$ the Dirac function and ∇ the usual gradient operator. In Eq. (9), first term corresponds to the regularization term (minimization of the final length) and second term to the maximisation of the alpha-divergence between p_{in} and p_{out}.

For fast implementation under Matlab© 2012, the AOS scheme formerly introduced in [Weickert 88] was used.

4.2 Parameters setting

As it can be noticed in Eq. (9), several parameters, namely β, ξ, σ and α influence the optimisation process.

Considering β and ξ, we arbitrarily set ξ to one and then empirically tuned β to have a sufficient "amount of energy" for the segmentation process to start and evolve. Main interest of the proposed method is to automatically balance the confidence in the divergence term of Eq. (9) using alpha-parameter and not being too dependent of β value.

σ value is empirically tuned to 0.1. A lower value does not bring much to the PDF estimation and a higher value results in a too important smoothing effect on the shape of the PDF (loss of information).

Finally, about alpha-parameter that can be seen as the key point of the proposed approach, we propose an automatic setting based on a joint optimization process with Eq. (9). More precisely, optimal value of alpha-parameter, α_{opti}, is obtained using a classic gradient descent such as to solve:

$$\alpha_{opti} = \underset{\alpha}{\operatorname{argmax}}\left(D_{\alpha}(p_{in} \,\|\, p_{out})\right) \quad , \quad (10)$$

Eq. (9) and Eq. (10) being optimized in turn. α_{opti} value is initialized to 1 in order to start from the classic KL-divergence that corresponds to Shannon context for which no prior information on the shape of the PDF to separate are taken into account. Main idea is to let the statistical discriminative properties arise from the iterative optimisation process of alpha parameter.

The corresponding proposed algorithm is the following one:

1. **Initialization**
   - $\tau = 0$
   - p_{in} and p_{out} (depends on active contour initialization)
   - $\alpha_{opti} \leftarrow \alpha_0$
2. **Optimization**
   While $\phi(\tau) \neq \phi(\tau - 1)$, do :
   (a) For $\alpha = \alpha_{opti}$:
   Iteration of convergence process of the curve ϕ
   p_{in} and p_{out} update
   (b) For fixed p_{in} and p_{out} :
   Iteration of optimization process for α
   α_{opti} value update
   (c) $\tau \leftarrow \tau + 1$
   End while

4.3 Experiments

4.3.1 Synthetic images

First of all, to illustrate the properties of the proposed method, we show the results obtained on a synthetic image (Fig. 7). The "peanut" binary shape is corrupted using a strong Gaussian noise such as the PSNR is only of 10dB. The segmentation process is initialized using a multiple circles strategy as illustrated Fig. 6a. Fig. 6b shows the segmentation result obtained with the KL-divergence and Fig. 6c with the proposed approach coupling the maximizations of the alpha-divergence and of alpha value.

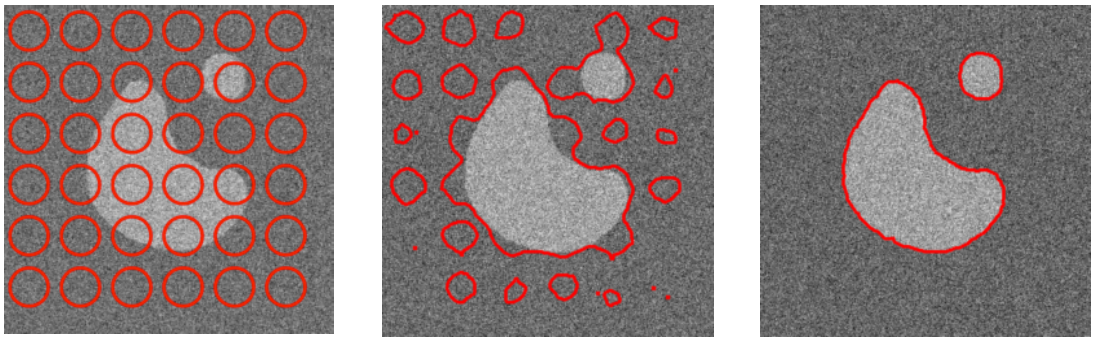

(a) (b) (c)

Fig. 7 Segmentation results: Comparison between KL-divergence based approach and our method. (a) Original noisy image (Gaussian noise) and initialization of the segmentation process, (b) Segmentation result with KL divergence, (c) Segmentation result with proposed approach (ξ=1, β=1, σ=*0.1*).

As it can be noticed, if KL-divergence fails because of the too strong amount of noise, even for Gaussian PDF, proposed method and strategy of optimization for alpha-value permit the obtaining of a satisfying segmentation. Fig. 7(b) shows that with KL divergence, the segmentation process finally stops in a local maximum that does not correspond to the desired segmentation. Optimizing the metric in parallel with the evolution of the active curve makes possible an adaptation to the statistic properties of the PDF all along the process. At convergence, final alpha-value is 0.5 in this particular case.

Fig. 8 illustrates performance of the proposed approach on a texture image computed from the Brodatz database. Again, a comparison between KL-divergence and our approach is shown.

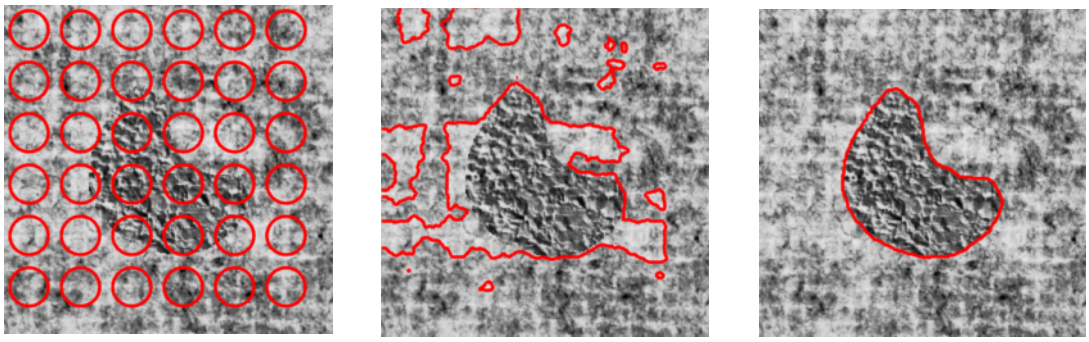

(a) (b) (c)

Fig. 8 Segmentation results: Comparison between KL-divergence based approach and our method. (a) Original texture image and initialization of the segmentation process, (b) Segmentation result with KL divergence, (c) Segmentation result with proposed approach (ξ=1, β=5, σ=*0.1*).

In that particular case, at convergence optimal alpha value is 0.4. Again, KL divergence fails to segment the peanut shape, being stuck into a local maximum whereas proposed approach leads to the right segmentation.

In terms of robustness, a first statistical evaluation of the final segmentation error (percentage of misclassified pixels) on the peanut shape of Fig. 7 was carried out. Tab. 1 summarizes obtained results.

Gaussian noise (10dB)	**Segmentation error (%)** Mean (standard-deviation)
KL-divergence ($\alpha=1$)	19.04 (3.4)
α_{opti}	0.35 (0.02)

Tab.1: Average segmentation error in percentage of misclassified pixels function of the strategy used for the setting of α parameter (KL or optimized).

Statistics of Tab. 1 were computed on 100 hundred independent experiments with a different realisation of the Gaussian noise in each case. Proposed method for each experiment outperforms the classic KL divergence and remains stable in terms of final segmentation results.

4.3.2 WCE image segmentation

In the following, we now consider application of the proposed approach to the segmentation of different type of structures in WCE images. Considering the initialization issue, we hypothesis that a pre-detection step permitted to automatically identify the barycentre of particular ROI identified as structure of interest by the learning-based approach of Silva et al [Silva 14] (see Fig. 3 for illustration). The initializing curve is a 20-pixels-diameter circle, which centre is the barycentre of the square in which the structure is included after the detection step.

For all the experiments, same values of hyper parameters were used ($\xi=1$, $\beta=10$, $\sigma=0.1$) except of course for alpha, which was optimized in accordance with the proposed strategy. As it can be noticed, in every case shown, the final segmentation is satisfying and makes possible the extraction of features including for instance, shape and texture ones. More precisely, as it can be noticed in Fig. 9, the maximisation of alpha-divergence is a flexible approach that could fit to different kind of segmentation structures acquired in challenging conditions. For instance, even in the case of polyp segmentation, which luminance characteristics are quite similar to the ones of the associated local background (Fig. 9(a-c)), the proposed segmentation approach makes delineation of the boundaries possible whereas usual approach like the Chan and Vese one, necessarily fail.

Fig. 9: WCE image segmentation using the proposed histogram-based active contour approach. (a) and (b) gastric polyps in Peutz-Jeghers syndrome (c) Colon sigmoid polyp, (d) Lymphangiectasia, (e) Small-bowel metastasis, (f) radiation enteritis (g) Angiodysplasia, (h) Lipoma, (i) Hypertrophied anal papilla. Indicated values of alpha correspond to the optimal value reach at convergence of the joint optimisation process.

Moreover, as illustrated in Fig. 9(d) and (f), even if lesions are diffused (like radiation enteritis), the alpha divergence criterion remains efficient to highlight some particular regions

of interest within the considered image. It is also possible to note that the best-obtained results of Fig. 9 correspond to value of α_{opti} lower than one, i.e. different from the asymptotic case $\alpha=1$ (KL divergence) often used in the particular framework of statistical based active contour.

To allow a visual comparison with KL-divergence, we considered some of the most challenging images (mainly polyps) of Fig. 9 and performed the segmentation using this similarity measure. Same initialisation and hyper parameters were used. Results are shown in Fig. 10.

Fig. 10: WCE image segmentation using histogram-based active contour approach with KL divergence. (a) Colon sigmoid polyp, (b) Gastric polyps in Peutz-Jeghers syndrome, (c) Hypertrophied anal papilla. Same initialisation and hyper parameters than those of previous experiments were chosen.

In each case, it can be noticed that the proposed method outperforms classic KL-based approach.

Finally, in Fig. 11, semi-automatic segmentation results are compared with the corresponding manual delineation performed by the clinicians using the "RatSnake" dedicated free software [Iakovidis 14].


03:08:50
20 Mar 10
JF
PillCam® SB

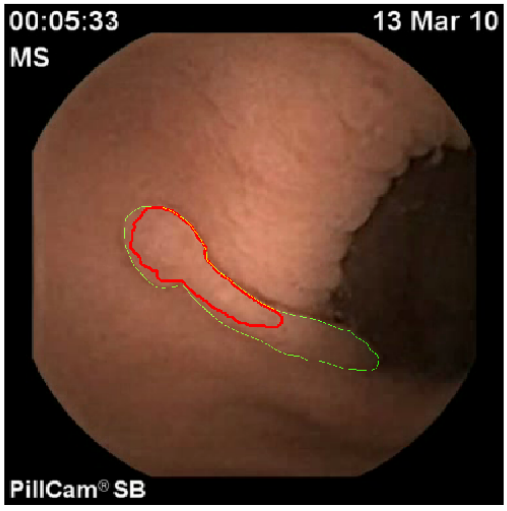
00:05:33
13 Mar 10
MS
PillCam® SB

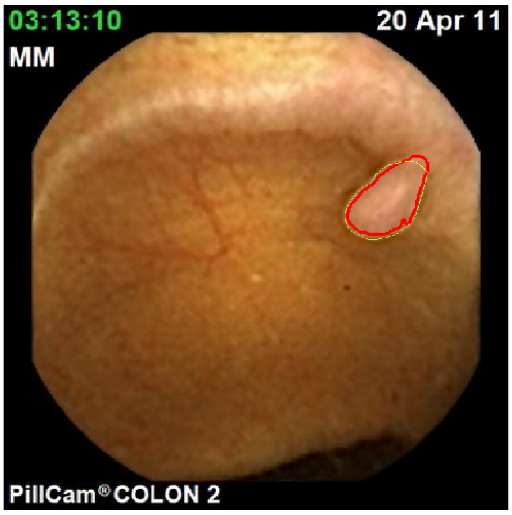
03:13:10
20 Apr 11
MM
PillCam® COLON 2


02:39:02
12 Apr 05
EF
Given®

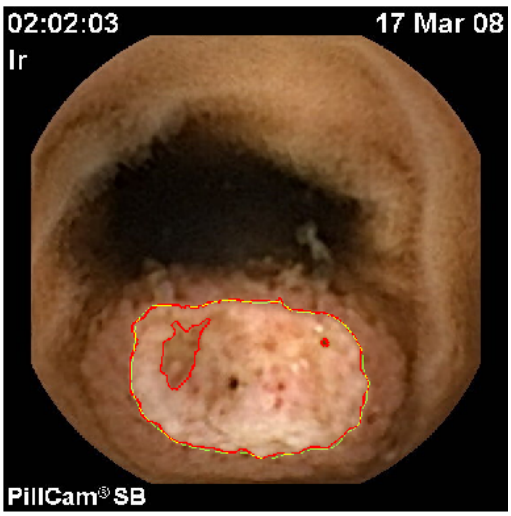
02:02:03
17 Mar 08
Ir
PillCam® SB

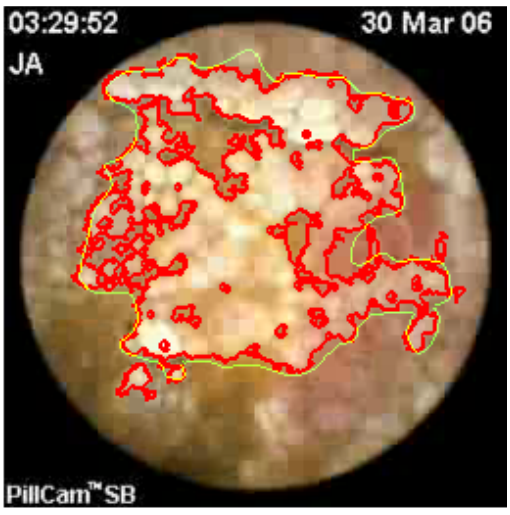
03:29:52
30 Mar 06
JA
PillCam™ SB

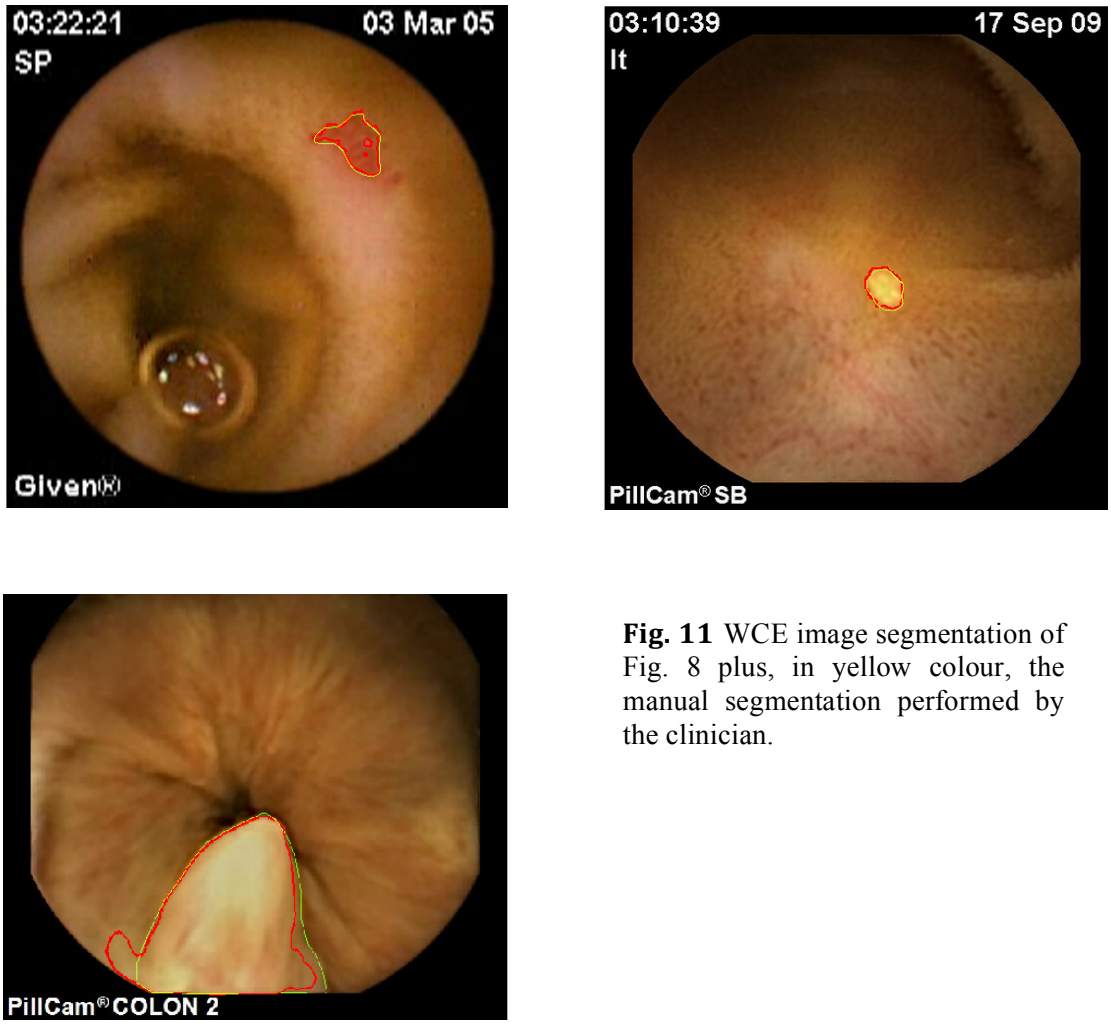

Fig. 11 WCE image segmentation of Fig. 8 plus, in yellow colour, the manual segmentation performed by the clinician.

We provide here visual results showing that, in most cases, the semi-automatic segmentation is very close from the clinician's one. In addition, in Tab. 2, for each case, the segmentation error is proposed (computed as the number of misclassified pixels compare to the manual-segmentation mask).

These quantitative results must be considered with care because some values that may be seen as "bad" ones (for instance with the Gastric polyp (b)) does not highlight the fact that the segmentation obtained with the semi-automatic proposed method is definitely of better interest than the one obtained with KL divergence. One can also notice that for particular cases like the "enteritis" image or the "metastasis" one, the clinician does not take into account the possible complex topology of the ROI to segment. Because, we use level-set algorithms, the obtained results can highlight particular topological properties that can be of real interest for further characterizations.

Image	Segmentation error (%)	
	Alpha-div	**KL**
(a) Gastric Polyps	<1	
(b) Gastric polyp	44.2	82.3
(c) Colon Sigmoïd polyp	1.2	~500
(d) Lymphangiectasy	<1	
(e) Metastasis	15.3	
(f) Radit Enteritis	14.7	
(g) Angioma	1.5	
(h) Lipoma	<1	
(i) Anal Papilla	11.2	10.3

Tab. 2: Average segmentation error in percentage of misclassified pixels with respect to the divergence used.

5 Conclusion and Discussion

In this article, a flexible statistical region-based active contour criterion has been presented for WCE image segmentation. Based on alpha-divergence similarity, this criterion, embedded into a maximisation scheme of the corresponding segmentation energy, shows a real flexibility regarding the particular type of data considered which are acquired in non usual conditions. The obtained results on a set of WCE images showed that the proposed method overcome the usual drawback of histogram-based method using KL divergence for similarity measure.

From a clinical point of view, we now need to improve the performance (robustness and reproducibility mainly) on a larger set of data. For this purpose, an acquisition campaign is currently on the run with the clinical partner of the project (APHP, Hôpital Lariboisière, Department of Gastroenterology, Paris Sorbonne Paris 7 University).

Prospective work in terms of image processing will focus on three main issues:

(i) To take into account colour features of WCE images that can be related to textural information;

(ii) To extract meaningful clinical parameters from the segmented area in order to better differentiate benign from malignant lesions;

(iii) To embed within the capsule the proposed approach, in order to make it compatible with real-time in situ processing.

Conflict of interest

The authors have not declared any conflicts of interest.

Acknowledgement

Part of this work was achieved in the framework of TERAFS project (EPSRC Grant EP/F013698/1).

References

[Amari 09] S. Amari. Alpha-Divergence is unique, belonging to both f-divergence and Bregman divergence classes. IEEE Transactions on Information Theory, pages 4925–4931, 2009.

[Aubert 03] G. Aubert, M. Barlaud, O. Faugeras & S. Jehan-Besson. Image segmentation using active contours: Calculus of variations or shape gradients?, SIAM J. Appl. Math., vol. 63, pages 2128–2154, 2003.

[Chan 01] T. F. Chan & L. A. Vese. Active Contours Without Edges. IEEE trans. on IP, vol. 10, no. 2, pages 266–277, February 2001

[Cichocki 10] A. Cichocki & Shun-ichi Amari. Families of Alpha- Beta- and Gamma-Divergences : Flexible and Robust Measures of Similarities. Entropy, vol. 12, no. 6, pages 1532–1568, 2010.

[Herbulot 07] A. Herbulot. Mesures statistiques non-paramétriques pour la segmentation d'images et de vidéos et minimisation par contours actifs. PhD thesis, Université de Nice Sophia-Antipolis, 2007.

[Hero 02] A.O Hero, B. Ma, O. Michel & J.D. Gorman. Alpha-Divergence for Classification, Indexing and Retrieval. Technical Report CSPL-328, University of Michigan, June 2002

[Iakovidis 14] D.K. Iakovidis, C. Smailis, T. Goudas, and I. Maglogiannis, "Ratsnake: A Versatile Image Annotation Tool with Application to Computer-Aided Diagnosis," The Scientific World Journal, vol. 2014, Article ID 286856, 12 pages, 2014. doi:10.1155/2014/286856

[J-Besson 03] Stéphanie Jehan-Besson. Modèles de contours actifs basés régions pour la segmentation d'images et de vidéos. PhD thesis, Université de Nice-Sophia Antipolis, 2003.

[Kass 88] M. Kass, A Witkin & D. Terzopoulos. Snakes : Active contour models. Int. J. Comput. Vision, vol. V1, no. 4, pages 321–331, January 1988.

[Lecellier 10] F. Lecellier, M.J. Fadili, S. Jehan-Besson, G. Aubert, M. Revenu & E. Saloux. Region-Based Active Contours with Exponential Family Observations. Journal of Mathematical Imaging and Vision, vol. 36, no. 1, pages 28–45, January 2010.

[Lecellier 14] F. Lecellier, S. Jehan-Besson, J. Fadili, Statistical region-based active contours for segmentation: an overview, IRBM, vol. 35, no. 1, pages 3-10, 2014.

[Meziou12] L. Meziou, A. Histace & F. Precioso. Alpha-divergence maximization for statistical region-based active contour segmentation with nonparametric PDF estimations. In Proceedings of International Conference on Accoustics, Speech and Signal Processing ICASSP, pages 861-864, Kyoto, Japon, March 2012.

[Moglia 09] A. Moglia, , A. Menciassi, A. Dario, and A. Cuschieri, Capsule endoscopy: progress update and challenges ahead, Nature reviews. Gastroenterology & hepatology, no. 6, pp. 352-362, June 2009.

[Osher 88] S. Osher & J. A. Sethian. Fronts Propagating with Curvature Dependent Speed: Algorithms Based on Hamilton-Jacobi Formulations. Journal of Comp. Phy., vol. 79, pages 12–49, 1988.

[Parzen 62] E. Parzen. On Estimation of a Probability Density Function and Mode. The Annals of Mathematical Statistics, vol. 33, no. 3, pages 1065–1076, 1962.

[Silva 14] J. Silva, A. Histace, O. Romain, X. Dray, B. Granado, Towards embedded polyp detection in WCE image, International Journal of Computer Assisted Radiology and Surgery, volume 9, no. 2 , pages 283-293, 2014

[Weickert 98] J. Weickert, B. M. Ter Haar Romeny & M. A. Viergever. Efficient and reliable schemes for nonlinear diffusion filtering. IEEE trans. on IP, vol. 7, no. 3, pages 398–410, March 1998.